Electronic Supplementary Information
Accounting for π–π Stacking Interactions in Mesoscopic Models of Conjugated Polymers

Vladimir Yu. Rudyak,*[a] Alexey A. Gavrilov,[a] Daria V. Guseva,[b] Shih-Huang Tung,[c] and Pavel V. Komarov[b,d]

Here we present additional information and computer simulation data on the morphologies of the systems under study. All parameters are expressed with using DPD units, viz., $m = 1$ (the mass of the DPD particles), $\sigma = 1$ (the unit of scale), $k_BT = 1$ (the unit of energy, T is absolute temperature, k_B is the Boltzmann constant), $\left(\frac{m\sigma^2}{k_BT}\right)^{1/2} = 1$ (the unit of time) [1].

S1. The repulsion parameter a_{AB} for the case of poly(3-hexylthiophene) (P3HT)

In order to calculate the repulsion constant a_{AB} [1]

$$a_{\mathrm{AB}} = a_0 + 3.497\chi_{\mathrm{AB}},$$

which determines repulsion interaction between A and B beads (the choice of parameter a_0 is described in subsection S2), it is necessary to calculate the Flory-Huggins interaction parameter χ_{AB} [2,3] of the alkyl chains with thiophene backbone. This can be done using the well-known relationship [4,5] between χ and the Hildebrant solubility parameters δ [5–7]:

$$\chi_{\mathrm{AB}} = v(\delta_A - \delta_B)/RT + \chi_S,$$

where v is the averaged molecular volume of beads, R is the gas constant, χ_{S} is the contribution of entropy to the free mixing energy, which for many mixtures is 0.34 [8,9]. It is a small correction in comparison with the first term.

Initially, the values for the Hildebrant parameters were estimated using the molecular dynamics method (MD) by calculating the cohesion energy density $E_{\mathrm{coh}}(N)$, according to the definition [5]

$$\delta(N) = (E_{\mathrm{coh}}(N)/V(N))^{1/2},$$

where $V(N)$ is the volume of the simulation cell, N is the number of molecules in the system under simulations. The calculations were performed using the molecular dynamics package LAMMPS [10], second-generation polymer-consistent force field (PCFF) [11–13], and the simulation protocol that we developed earlier [14,15]. The PCFF was validated in the case of amorphous thiophene by Zhang et al. [16,17] The solubility parameter was calculated for the following compounds: C_4H_9, C_5H_{12}, C_6H_{14}, thiophene, polythiophene (PTH), and P3HT. In the case of polythiophene and P3HT, we constructed short oligomer chains built from 4 monomers. To increase the accuracy of calculations, several samples were constructed for each molecular system containing N = 4–105 molecules. The results for $\delta(N)$ were extrapolated to the case when $N \to \infty$. To check the obtained results, we used estimates for δ done in the framework of Askadskii method [18] and data taken from the literature. Obtained results for considered substances are placed in Table S1.

As can be seen from Table S1, for all alkanes there is an acceptable agreement between the MD results, estimates according to the Askadskii method, and data from literary sources. In the case of the thiophene and polythiophene, a strong discrepancy between theoretical results and the experimental data is seen. This might be explained by the fact that the Askadskii method and force field used in MD simulation underestimated the intermolecular interaction of thiophene rings.

Unfortunately, there are very few publications on the solubility of polythiophene. Nevertheless, taking into account the fact that polythiophene is soluble in solvents such as methylpyrrolidone (NMP), dimethylformamide (DMF), and dimethylsulfoxide (DMSO) with solubility parameters of 22.9 MPa$^{1/2}$, 24.8 MPa$^{1/2}$, and 26.6 MPa$^{1/2}$, respectively [19], polythiophene cannot have the same solubility parameter as P3HT. Since molecular dynamics gives an acceptable estimate of the solubility parameter for alkanes and P3HT, we used these values to estimate δ in the case of polythiophene by using the simple rule [7]

$$\delta^2_{\mathrm{P3HT}} = (V_{\mathrm{PTH}}\delta^2_{\mathrm{PTH}} + V_{\mathrm{C6H14}}\delta^2_{\mathrm{P3HT}})/V_{\mathrm{P3HT}},$$

where $V_{\mathrm{PTH}}/V_{\mathrm{P3HT}}$ and $V_{\mathrm{C6H14}}/V_{\mathrm{P3HT}}$ are relative molar volumes of thiophene ring and alkyl chain as parts of the whole P3HT monomer. In the estimates, we made a correction of molar volume for C_6H_{14} because the alkyl chain in P3HT contains one less hydrogen atom. For PTH, we obtained a value of $\approx$ 21.1 Mpa$^{1/2}$, which is slightly less for the experimental range [19]. In our opinion, this is mainly

[a] Faculty of Physics, Lomonosov Moscow State University, Leninskie Gory, 1-2, Moscow 119991, Russia.
[b] Nesmeyanov Institute of Organoelement Compounds, Russian Academy of Sciences, Vavilova st., 28, Moscow 119991, Russia.
[c] Institute of Polymer Science and Engineering, National Taiwan University, Taipei 10617, Taiwan.
[d] Tver State University, Sadovyj per., 35, Tver 170002, Russia.

	Density ρ [g/cm^3]	δ [MPa$^{1/2}$]	V_m [cm^3/Mol]	δ [MPa$^{1/2}$]	Density ρ [g/cm^3]	δ [MPa$^{1/2}$]
	Ascadskii			MD	Literature data	
C_5H_{12}	0.677	15.4	107	14.5 ± 0.1	0.62[5,21]	14.5[5], 14.3[21]
C_6H_{14}	0.688	14.5	125	14.7 ± 0.1	0.66[5,21]	14.90[5], 14.8[21]
C_8H_{18}	0.702	15.5	163	15.0 ± 0.2	0.70[5,21]	15.5[5], 14.0[21]
Thiophene	0.98	17.6	85.8	16.9 ± 0.3	1.06[22]	20.59[23,24]
PTH	1.4	18.9	58.7	17.5 ± 0.2 ($\rho = 1.2$) 20.1 ± 0.5 ($\rho = 1.4$)	1.2[25]	22.9–26.6[19]
P3HT	1.08	17.3	154	17.4 ± 0.2	1.05–1.1[19,26,27]	20[28]; 19.05[29]; 19.0[30]

Table S1 Characteristics of the substances used to parameterize the DPD model: density, molar volume V_m, and solubility parameters δ.

due to the fact that the constructed P3HT samples have an amorphous structure, while it is known that this polymer has a fairly high degree of crystallinity (60-70%) and the energy cohesion of the system should be higher. Therefore, to determine the region in the state diagram (Fig. 3a) of the corresponding P3HT, we used the experimental values for the solubility parameters P3HT and hexane (collected in Table S1). As a result, we obtained $\delta_{\text{PTH}} \approx 24.6$ MPa$^{1/2}$ which belongs to the experimental range of solubility parameters of good solvents for polythiophene (22.9–26.6 MPa$^{1/2}$)[19]. This value and the value 14.85 MPa$^{1/2}$ were used as δ_A and δ_B, respectively, to estimate χ_{AB} and a_{AB}. The obtained value $\chi_{AB} = 2.5$ corresponds to P3HT on the phase diagrams in Fig. 2 and Fig. 3a.

It should be noted that in[20] the obtained value for χ_{AB} was equal to 1.5, which is less than our result. This difference can be explained by the fact that in[20] the authors used the value 16.22 MPa$^{1/2}$ for δ_A obtained for thiophene with the molecular dynamics, which is very different from the average experimental value we used. The latter correlates well with our result for thiophene, see Table S1.

S2. Choice of the repulsion parameter a_0

Conventional DPD simulations use soft potential with typical values of repulsion parameter a_0 around 25. In our model, we use higher values of repulsion parameters ($a_0 = 100$) and correspondingly higher bond and angle strengths ($K_b = 50$, $K_A \in [3;24]$). This set of parameters leads to much harder potential that is still much softer than Lennard-Jones one. This is done for two reasons. First, high repulsion in DPD in combination with short equilibrium bond length ($l_b = 0.5$) and strong bonds ($K_b = 50$) results in non-phantom behavior of polymer chains[31,32]. Despite the fact that the repulsion potential at $r = 0$ is finite, the barrier is too high in comparison to k_BT and can not be passed. In turn, non-phantom dynamics of the chains leads to more physical behavior of the system, crucial for complex soft matter phenomena. Second, the outcome of the dynamic bonding procedure is entirely dependent on the ability of DPD beads to come close to each other. Softer potential (like $a_0 = 25$) leads to the formation of many non-physical dynamic bonds due to the allowance of deep interpenetration of the beads. It can be solved by complex geometrical limitations in the bond formation procedure, but using the hard potential is simpler and more physical way to avoid abnormal behaviour of dynamic bonding procedure.

S3. Morphology of representative structures

Below we present examples of detailed visualization for morphologies of simulated samples schematically shown in Fig. 3(b-e) of the manuscript. The main chain beads (corresponding to thiophene rings) are represented by thick blue tubes, the side chain beads (alkyl chains) are represented by thin gray tubes.

S4. Ordering parameter in the obtained morphologies

Ordering parameter was calculated as $P = \frac{1}{2}\langle 3\cos(\bar{b}_i, \langle \bar{b}_i \rangle_{R_{cut}}) - 1 \rangle_i$, where $\bar{b}_i$ is the direction of i-th bond, $\langle \bar{b}_i \rangle_{R_{cut}}$ is the average direction of all main chain bonds in radius R_{cut} from i-th bond, and averaging for $P(\langle ... \rangle_i)$ is calculated by all main chain bonds in the system. For each phase type, P was additionally averaged over ten conformations at frequency of 10^7 steps. Fig. S6 shows the calculated order parameter for various systems as a function of R_{cut}. Values of P at $R_{cut} \approx 3$ show the local nematic ordering of the chains, values at $R_{cut} > 15$ show overall nematic ordering.

S5. Effect of main chain length

We equilibrated systems of main chain lengths equal to 10, 20, and 40 monomers to analyze the effect of chain length on the ordering of the system. All simulations were produced with $30 \times 30 \times 30$ simulations box (81000 particles) with $K_a = 12$ and $\Delta a = 10$ ($\chi_{AB} = 3$).

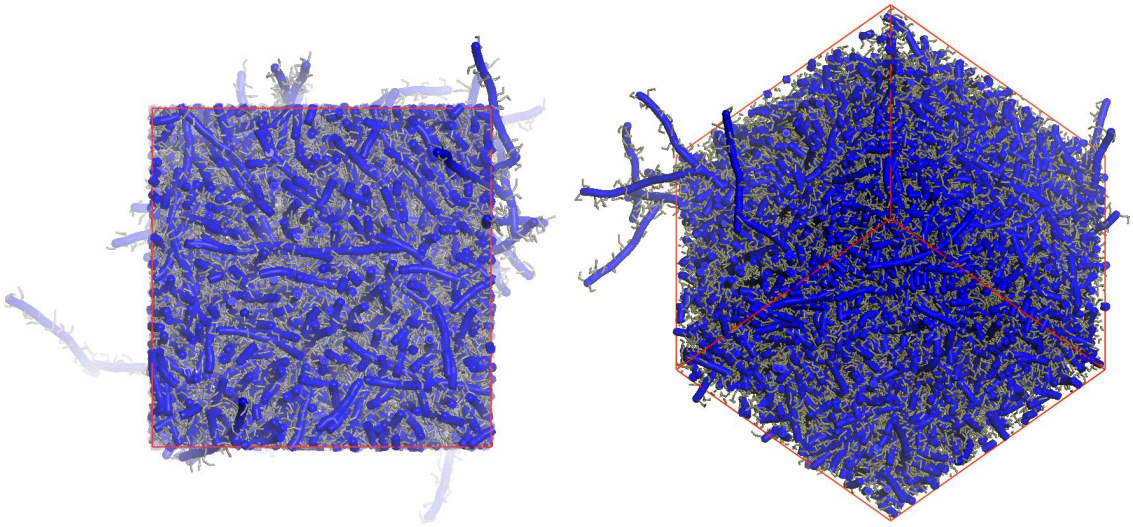

(a) (b)

Fig. S1 Disordered morphology (a) XY axis side view; (b) isometric view. $K_A = 12$, $\chi_{AB} = 0$, $p_{\mathsf{create}}/p_{\mathsf{break}} = 2$.

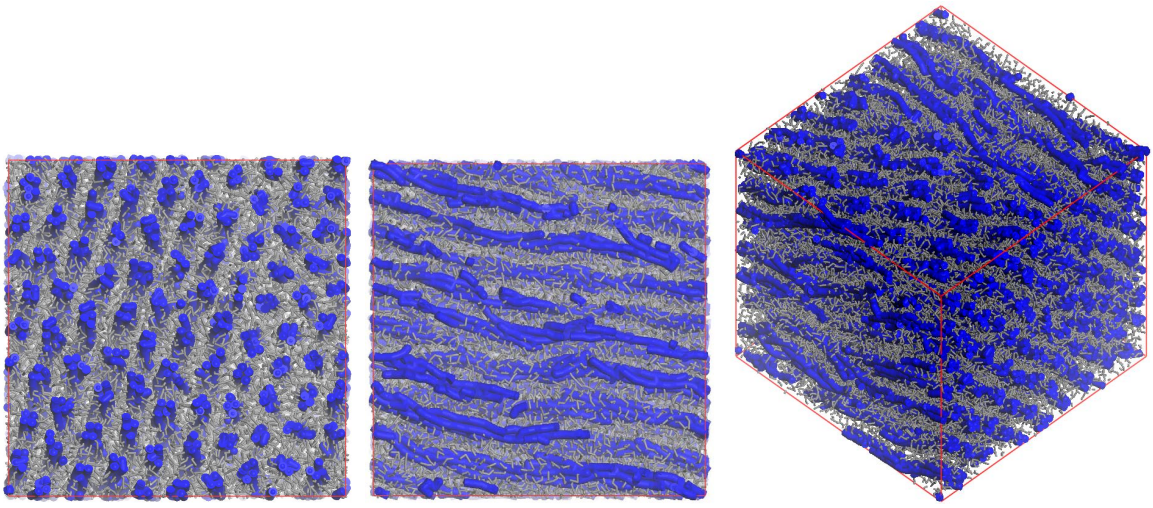

(a) (b) (c)

Fig. S2 Hexagonal-packed cylinder structure (a) XY axis side view; (b) XZ axis side view; (c) isometric view. $K_A = 12$, $\chi_{AB} = 5.7$, $p_{\mathsf{create}}/p_{\mathsf{break}} = 2$.

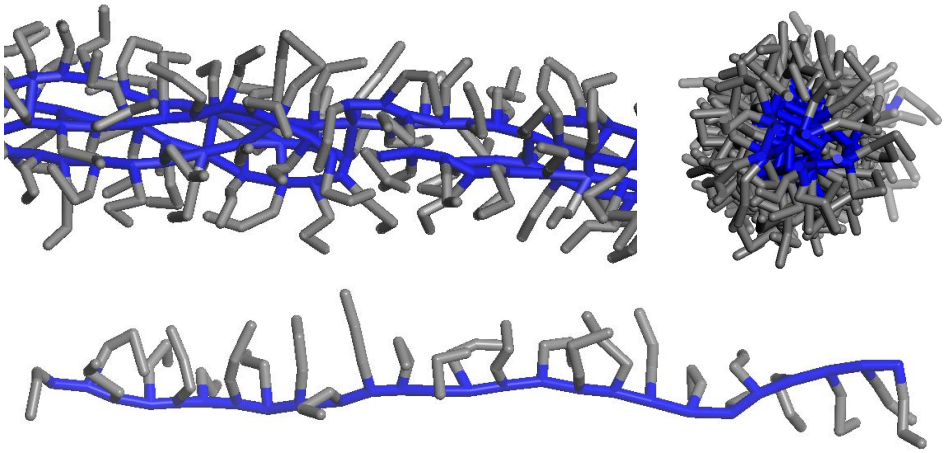

Fig. S3 The structure of the cylindrical aggregate (a) side view; (b) top view; (c) the morphology of a single chain inside the cylindrical aggregate.

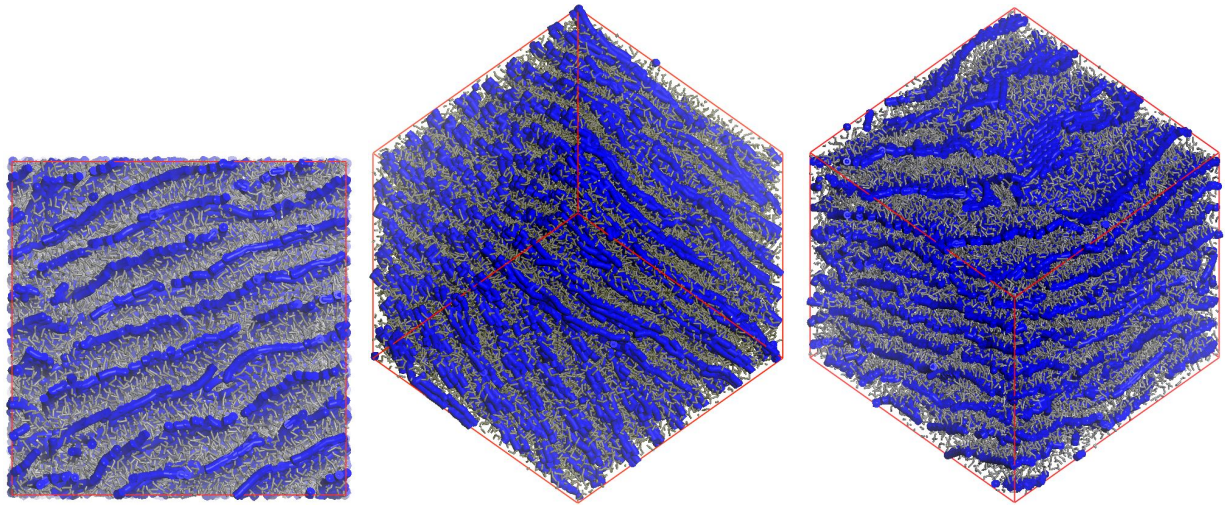

(a) (b) (c)

Fig. S4 Lammelar structure (a) XY axis side view; (b) isometric view 1; (c) isometric view 2. $K_A = 12$, $\chi_{AB} = 5.7$, $p_{\mathsf{create}}/p_{\mathsf{break}} = 4$.

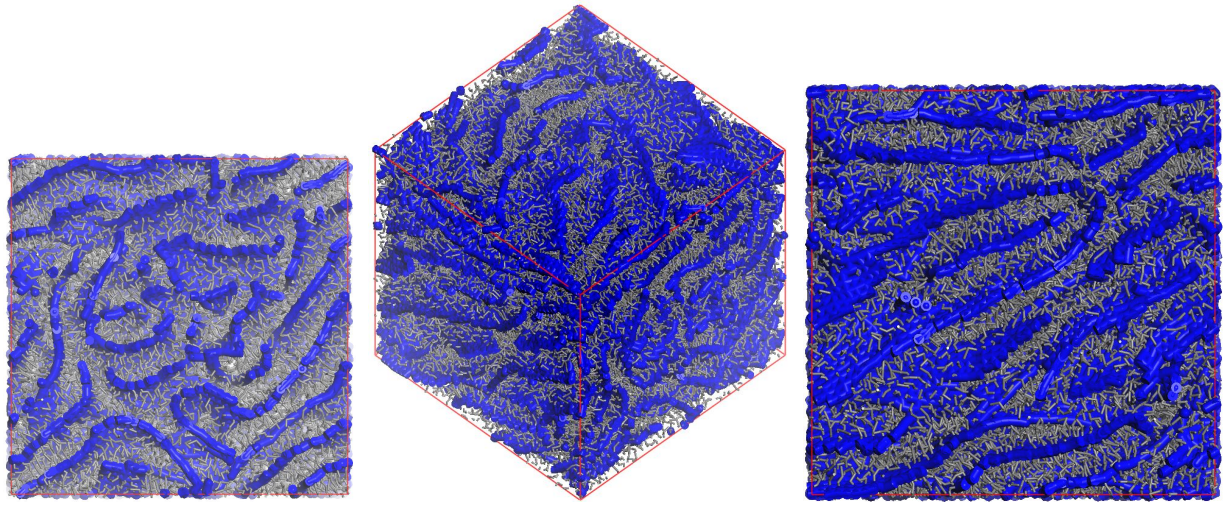

(a) (b) (c)

Fig. S5 Disordered lamellar structure (a) XY axis side view; (b) isometric view; (c) XZ axis side view. $K_A = 12$, $\chi_{AB} = 5.7$, $p_{\mathsf{create}}/p_{\mathsf{break}} = 10$.

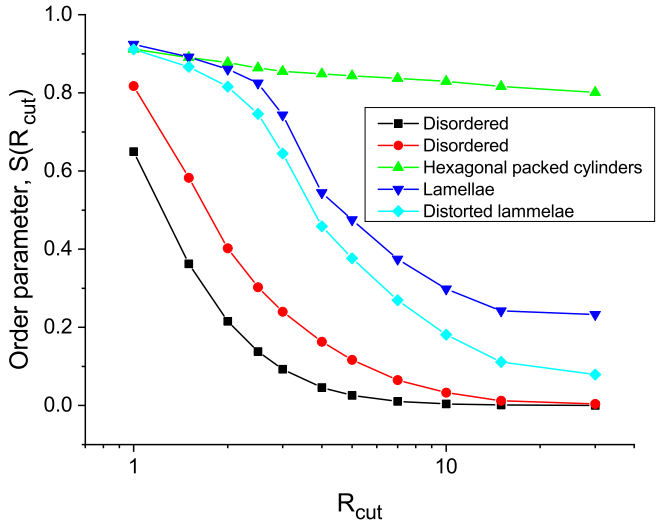

Fig. S6 Dependence of the order parameter P on the cutoff radius R_{cut} for various morphologies observed in the system: disordered (black squares, $K_A = 3$, $p_{\text{create}}/p_{\text{break}} = 1$, $\chi_{\text{AB}} = 0$), disordered (red circles, $K_A = 24$, $p_{\text{create}}/p_{\text{break}} = 1$, $\chi_{\text{AB}} = 0$), hexagonal packed cylinders (green triangles, $K_A = 12$, $p_{\text{create}}/p_{\text{break}} = 2$, $\chi_{\text{AB}} = 6$), lamellae (blue down triangles, $K_A = 12$, $p_{\text{create}}/p_{\text{break}} = 4$, $\chi_{\text{AB}} = 12$), and distorted lamellae (light blue rhombs, $K_A = 12$, $p_{\text{create}}/p_{\text{break}} = 10$, $\chi_{\text{AB}} = 12$).

The resulting phase diagram is shown in Fig. S7. Short chains ($n = 10$) form only disordered and disordered lamellae phases due to its higher mobility. At the same time, the same diagram of states was obtained for 20-mer and 40-mer chains.

Fig. S8 shows snapshots of $n = 10$ system after 200 million steps equilibration. While at $p_{\text{create}}/p_{\text{break}} = 0.25$ and above, there is no ordering in the system, the higher value While at $p_{\text{create}}/p_{\text{break}} = 0.10$ still results in distorted lamellae. Snapshots for system with $n = 40$ after 200–250 million steps equilibration are shown in Fig. S9. While both cylinders and lamellae are not perfectly aligned across the simulations box, the phase type is clearly visible on these snapshots.

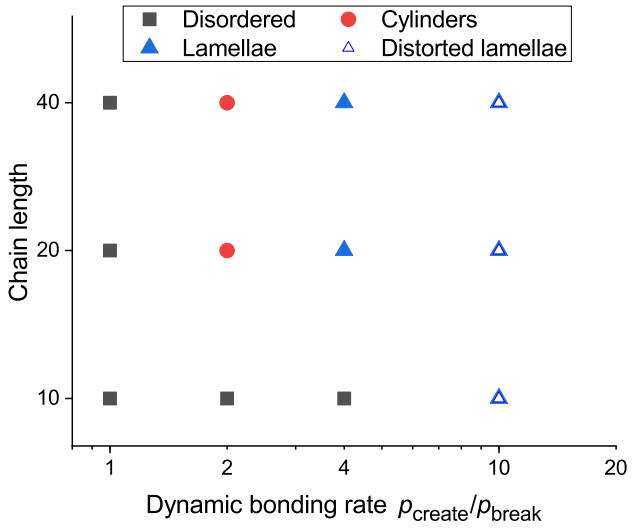

Fig. S7 Phase diagram of equilibrated systems at various dynamic bonding rate $p_{\text{create}}/p_{\text{break}}$ and main chain length.

Notes and references

1 R. D. Groot and P. B. Warren, The Journal of Chemical Physics, 1997, **107**, 4423–4435.
2 P. J. Flory, J. Chem. Phys., 1941, **9**, 660–661.
3 M. L. Huggins, J. Chem. Phys., 1941, **9**, 440–440.
4 X. D. Guo, L. J. Zhang, Z. M. Wu and Y. Qian, Macromolecules, 2010, **43**, 7839–7844.
5 C. M. Hansen, Hansen Solubility Parameters: A User's Handbook, Second Edition, Taylor Francis, 2007.

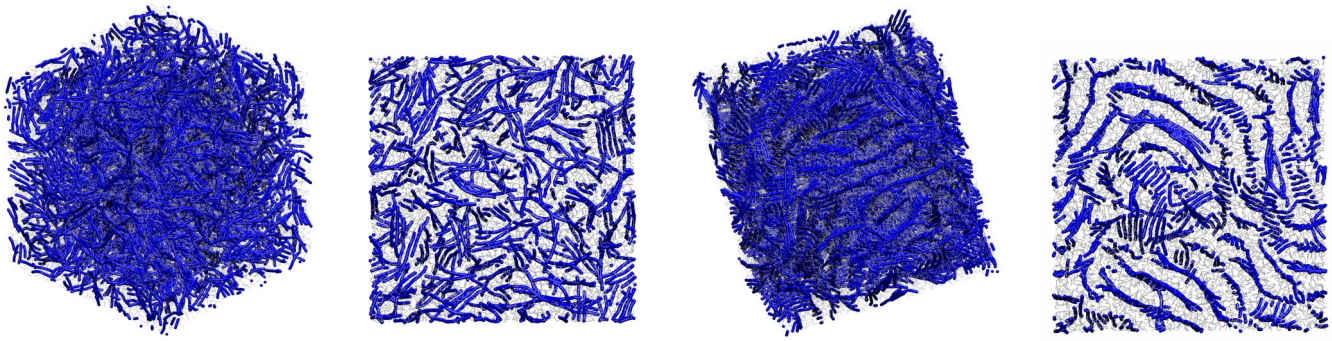

(a) (b) (c) (d)

Fig. S8 Snapshots of system with main chain length $n = 10$ at dynamic bonding rates $p_{\mathsf{create}}/p_{\mathsf{break}}$ equal to (a,b) 0.25, and (c,d) 0.1.

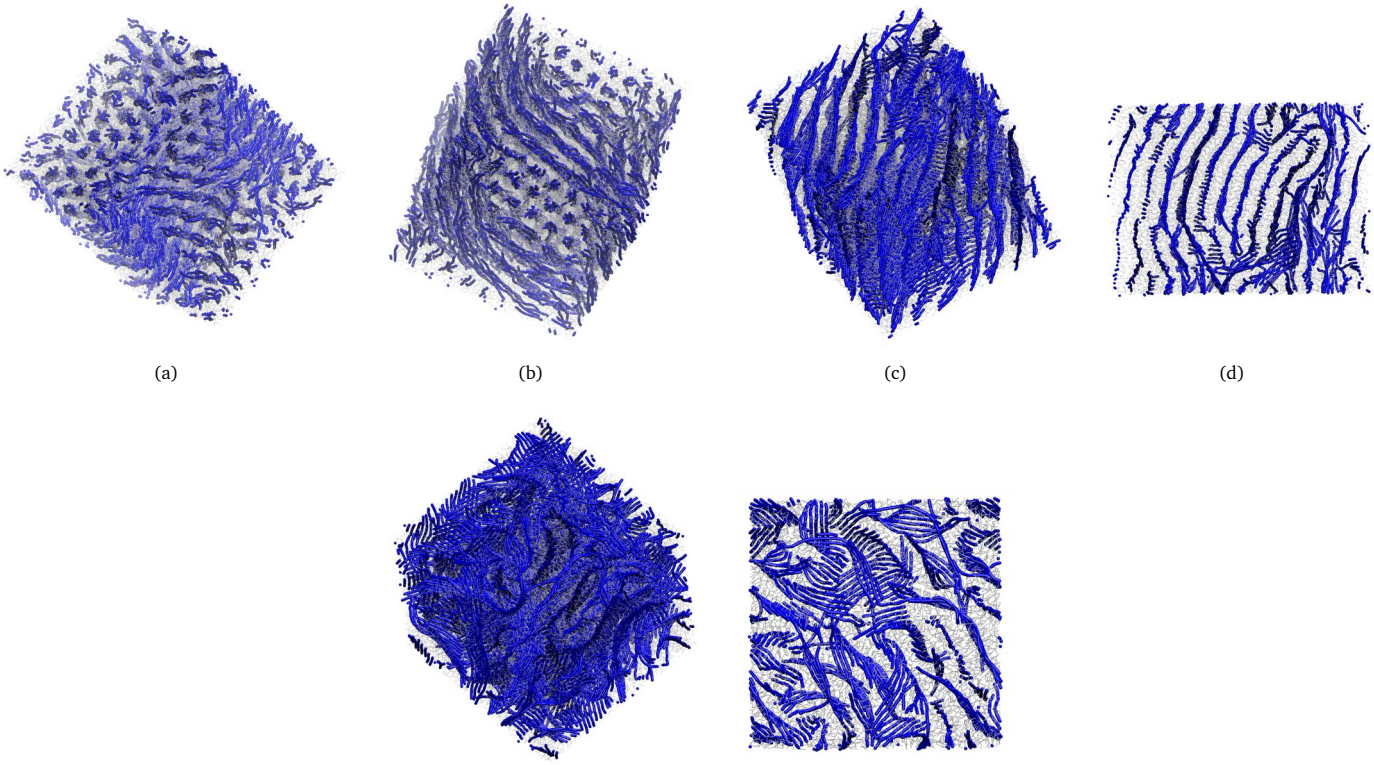

(a) (b) (c) (d)

(e) (f)

Fig. S9 Snapshots of system with main chain length $n = 40$ at dynamic bonding rates $p_{\mathsf{create}}/p_{\mathsf{break}}$ equal to (a,b) 0.5, (c,d) 0.25, and (e,f) 0.1.

6 L. I. Stiel, AIChE Journal, 1971, **17**, iv–iv.
7 C. Reichardt, Solvents and Solvent Effects in Organic Chemistry: Edition 3, John Wiley Sons, 2006.
8 E. Spohr, P. Commer and K. A. A., J. Phys. Chem. B., 2002, **106**, 10560–10569.
9 M. W. Verbrugge, R. F. Hill, Schneider and E. W., AIChE Journal, 1992, **38**, 93–100.
10 S. Plimpton, Journal of Computational Physics, 1995, **117**, 1–19.
11 H. Sun, S. J. Mumby, J. R. Maple and A. T. Hagler, J. Am. Chem. Soc., 1994, **116**, 2978–2987.
12 H. Sun, Macromolecules, 1995, **28**, 701–712.
13 H. Sun, S. Mumby, J. Maple and A. Hagler, J. Phys. Chem., 1995, **99**, 5873–5882.
14 P. V. Komarov, I. N. Veselov and P. G. Khalatur, Polymer Science Series A, 2010, **52**, 191–208.
15 A. A. Markina, V. A. Ivanov, P. V. Komarov, A. R. Khokhlov and S.-H. Tung, J. Phys. Chem. B., 2017, **121**, 7878–7888.
16 G. Zhang, Y. Pei, J. Ma, K. Yin and C.-L. Chen, The Journal of Physical Chemistry B, 2004, **108**, 6988–6995.
17 G. Zhang, J. Ma and J. Wen, The Journal of Physical Chemistry B, 2007, **111**, 11670–11679.
18 A. A. Askadskii, Computational Materials Science of Polymers, Cambridge Int Science Publishing, 2011.
19 S. J. Lee, J. M. Lee, I. W. Cheong, H. Lee and J. H. Kim, Journal of Polymer Science. Part A, Polymer Chemistry, 2008, **46**, 2097–2107.
20 C. Du, Y. Ji, J. Xue, T. Hou, J. Tang, S.-T. Lee and Y. Li, Sci. Rep., 2015, **5**, 16854–13.
21 G. Wypych, Handbook of Solvents, ChemTec Publishing, 2001.
22 F. Ullmann, Thiophene in Ullmann's Encyclopedia of Industrial Chemistry, Wiley, 2000.
23 C. Panayiotou, Physical Chemistry Chemical Physics: PCCP, 2012, **14**, 3882–3908.
24 Q.-N. Zhu, Q. Wang, Y.-B. Hu and X. Abliz, Molecules, 2019, **24**, 1346–16.
25 S. Nejati, T. E. Minford, Y. Y. Smolin and K. K. Lau, ACS Nano, 2014, **8**, 5413–5422.
26 G. M. Newbloom, K. M. Weigandt and D. C. Pozzo, Soft Matter, 2012, **8**, 8854–8864.
27 A. Lefrancois, B. Luszczynska, B. Pepin-Donat, C. Lombard, B. Bouthinon, J.-M. Verilhac, M. Gromova, J. Faure-Vincent, S. Pouget, F. Chandezon, S. Sadki and P. Reiss, Sci. Rep., 2015, **5**, 7768–8.
28 F. Machui, S. Abbott, D. Waller, M. Koppe and C. J. Brabec, Macromolecular Chemistry and Physics, 2011, **212**, 2159–65.
29 D. T. Duong, B. Walker, J. Lin, C. Kim, J. Love, B. Purushothaman, J. E. Anthony and T. Nguyen, Polymer Physics, 2012, **50**, 1405–1413.
30 S. Lee, H. Jeon, M. Jang, K.-Y. Baek and H. Yang, ACS Appl. Mater. Interfaces, 2015, **7**, 1290–1297.
31 D. V. Guseva, V. Y. Rudyak, P. V. Komarov, A. V. Sulimov, B. A. Bulgakov and A. V. Chertovich, Journal of Polymer Science Part B: Polymer Physics, 2017, **56**, 362–374.
32 V. Y. Rudyak, A. A. Gavrilov, E. Y. Kozhunova and A. V. Chertovich, Soft Matter, 2018, **14**, 2777–2781.